Multiple Dirac fermions from a topological insulator and graphene superlattice

Hosub Jin, Jino Im, Jung-Hwan Song, and Arthur J. Freeman

Phys. Rev. B **85**, 045307 — Published 9 January 2012

DOI: 10.1103/PhysRevB.85.045307

Multiple Dirac Fermions from a topological insulator and graphene superlattice

Hosub Jin,[1,*] Jino Im,[1] Jung-Hwan Song,[1,†] and Arthur J. Freeman[1]

[1] *Department of Physics and Astronomy, Northwestern University, Evanston, Illinois 60208, USA*

Graphene and three-dimensional topological insulators are well-known Dirac materials whose bulk or surface states are governed by Dirac equations. They not only show good transport properties, but also carry various quanta related to the geometrical phase such as charge/spin/valley Hall conductances. Therefore, it is great challenge to combine the two Dirac materials together, realizing multiple Dirac fermions. By using first-principles density functional theory calculations, we demonstrate such a system built from topological insulator-band insulator-graphene superlattice structures. Hexagonal boron nitride is proposed as an ideal band insulating material in gluing graphene and topological insulators, providing a good substrate for graphene and a sharp interface with a topological insulator. The power factors for p-type doping are largely enhanced due to the charge conducting channels through the multiple Dirac cones. The systems characterized by the coexistence of the topologically protected interfacial and graphene Dirac cones can pave the way for developing integrated devices for electronics, spintronics and valleytronics applications.

Graphene and topologically protected surface states of three-dimensional topological insulators show similar low energy excitations - so called Dirac fermions - described by a (2+1)-dimensional Dirac equation[1–4]. Considering its bipartite structure of honeycomb lattice and spin degeneracy, graphene has 4 Dirac cones at the K and K′ points in the hexagonal Brillouin zone. On the other hand, topological surface states are localized in the two-dimensional plane with a finite width where the topological phase, designated as Z_2 invariants[5–8], changes, and have an odd number of Dirac cones. Both materials have attracted great attention for their novelty and applicability. Due to the underlying chirality of pseudospin or spin in each Dirac cone, both of them show high mobility and good transport properties[9–11] and carry many different degrees of freedom: graphene has charge and valley channels which are usable for electronics and valleytronics[12], respectively, and topological surface states have not only charge but also spin conducting channels for spintronics applications.

Most interestingly, combining two different Dirac fermions might open an opportunity for multi-functional devices which possess many back-scattering-free conducting channels carrying various physical quantities. Such systems can be realized in layered structures composed of a topological insulator (TI) and graphene separated by a band insulator (BI) where the BI layer possibly makes a discontinuity of the Z_2 invariants from 1 to 0, resulting in topologically protected surface states. Two Dirac cones from the TI/BI interface and graphene can behave independently due to the blocking band insulator layer which prevents the interaction between them. Moreover, multiple copies of Dirac cones are accessible in superlattice structures[13] where the two-dimensional layered structures of TI, BI, and graphene are repeated along the perpendicular direction. These superlattice structures can provide multiple conducting channels of Dirac cones with high mobility and various physical quantities, which are proportional to the number of layers. If we keep the TI layer thickness as thin as several nanometers, we can not only realize the densely populated Dirac cone channels, but also minimize the bulk conductivity due to almost unavoidable defects.

By using a first-principles density functional approach, we suggest TI/BI/graphene/BI superlattice structures which simultaneously show two kinds of Dirac fermions, one from graphene and the other from the TI/BI interface. The most important thing in materializing these systems is to find an appropriate BI material; it should have a large band gap to make a sharp interface with TI, and weakly interact with graphene to preserve good physical properties of the graphene Dirac cone. Here, we use hexagonal BN (hBN) and $PbBi_2Se_4$ as topologically trivial and non-trivial insulators, respectively[14,15]. $PbBi_2Se_4$ is a three-dimensional TI with one of the largest bulk band gaps (0.4eV) among three-dimensional TI and its lattice constants agree well with graphene, within 2%. hBN is a large gap BI (5.97eV) and its layered geometry is appropriate for designing supperlattice structures. More importantly, hBN was recently used as a substrate for high quality graphene devices[16,17], which play a crucial role in gluing the TI with graphene. The composite layered structures suggested here are applicable in two-dimensional thin films and three-dimensional bulk devices. As an example of utilizing charge conducting channels of multiple Dirac cones in TI/BI/graphene/BI superlattice structures, we also demonstrate thermoelectric properties such as Seebeck coefficients and power factors, showing a great improvement for p-type doping. Recent experiments on good quality TI thin films using various growth technique might be useful to realize the suggested configurations here[18–20].

First-principles calculations employing the full potential linearized augmented plane wave method[21] within the local density approximation were performed. The core states and the valence states were treated fully relativistically and scalar relativistically, respectively; SOC was included by a second variational procedure[22]. The in-plane lattice constants of the superlattice structures were set to the experimental values of $PbBi_2Se_4$, and the c-axis lattice constant and the internal coordinates were fully optimized. For $\mathbf{k}$-space integrations, a 13×13×1

mesh of special **k**-points was used in the irreducible Brillouin zone wedge. The energy cutoffs for the interstitial plane wave basis and the star functions were 21.2 and 100.0Ry. The muffin-tin radii of Pb, Bi, Se, B, N, and C were 2.8, 2.7, 2.5, 1.1, 1.4, and 1.2 bohr, respectively. To determine the Seebeck coefficient and the power factors, Boltzmann's equation is employed within the constant relaxation time approximation. The thermoelectric transport coefficients of S and σ can, therefore, be calculated as

$$\mathbf{L}^{(\nu)} = e^2\tau \int \frac{d\epsilon d\mathbf{k}}{8\pi^3} \left(-\frac{\partial f_0}{\partial \epsilon}\right) (\epsilon-\mu)^\nu \delta(\epsilon-\epsilon_\mathbf{k}) \mathbf{v_k}\mathbf{v_k}$$

$$\sigma = \mathbf{L}^{(0)},\ \mathbf{S} = -\frac{1}{eT}(\mathbf{L}^{(0)})^{-1}\mathbf{L}^{(1)}$$

where e, τ, f_0, and $\mathbf{v_k}$ denote the electrical charge, relaxation time, Fermi-Dirac distribution function, and group velocity, respectively. Different carrier concentrations for the transport coefficient calculations were treated within the rigid band model. The proper convergence of the calculation of the transport properties is achieved with a 101x101x1 mesh of **k**-points in the Brillouin zone, which corresponds to 901 **k**-points in the irreducible Brillouin zone.

$PbBi_2Se_4$ has a rhombohedral unit cell and a layered structure stacked along the c-axis of the hexagonal lattice, and consists of seven atoms in one septuple layer. As denoted previously, the difference of the in-plane lattice constants between $PbBi_2Se_4$ and graphene is small, and the 1×1 unit cell of $PbBi_2Se_4$ matches well with $\sqrt{3}\times\sqrt{3}$ graphene and hBN. The hexagonal center of hBN is placed on top of the outermost Se atoms at the TI/BI interfacial region. hBN layers have A-A' stacking where the B atom is located on top of N and vice versa. Within the superlattice structures, the graphene monolayer is laid in between the BI layers of hBN, and they show an A-B-A stacking sequence where one carbon atom is sandwiched by B atoms above and below, and the other carbon is located on the hexagon center of hBN, which is energetically favorable. Under these circumstances, the sublattice symmetry of graphene is broken, resulting in a gap at the Dirac point.

$PbBi_2Se_4$ is composed of a septuple layer unit and the interlayer coupling between neighboring septuple layers is mainly due to van der Waals type interactions. An insulating block of hBN layers is naturally placed between the septuple layers (Fig.1(a)), making $(PbBi_2Se_4)_m/(h\text{BN})_n$ superlattice structures where m and n are the number of layers of $PbBi_2Se_4$ and hBN, respectively. Here we fix m=3 in the TI layer, and find the minimum thickness of hBN for the blocking BI region at which the interfacial Dirac cones at each TI/BI boundary are established. For n=1, there is an interfacial state distinguished from the bulk states but it has a small but finite gap of 25meV at the Γ point in Fig.1(c), which does not correspond to the topologically protected gapless state connecting the inverted conduction and valence bands. The monolayer hBN does not make a discontinuity of the Z_2 invariants;

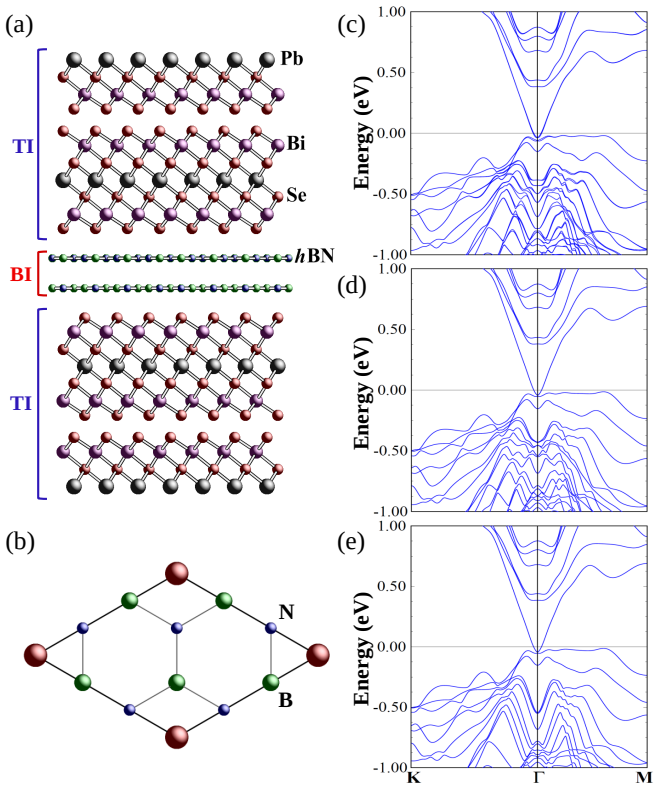

FIG. 1. (Color Online) Crystal structure of the $(PbBi_2Se_4)_3/(h\text{BN})_2$ superlattice: (a) side-view and (b) top view where the 1×1 unit cell of $PbBi_2Se_4$ and the $\sqrt{3}\times\sqrt{3}$ unit cell of hBN are overlapped. Electronic band structures of $(PbBi_2Se_4)_3/(h\text{BN})_n$ superlattice with (c) n=1 and (d) n=2, and (e) the $(PbBi_2Se_4)_3$ pristine slab. The similarity between (d) and (e) shows that $(h\text{BN})_2$ layer plays the same role as the vacuum.

in other words, the band insulating barrier produced by the hBN monolayer is not enough to prevent the interaction between neighboring TI layers through the barrier, resulting in a small gap in the interfacial Dirac cone. However, just after increasing n by 2, a gapless Dirac fermions appears at around the Γ point in Fig.1(d) as direct evidence of the alternating Z_2 invariants, thus multiple Dirac cones from each interface between TI and BI are accessible in this $(PbBi_2Se_4)_3/(h\text{BN})_2$ superlattice geometry. Considering the similarity of band structures between the TI/BI superlattice and the 3 septuple layers of the $PbBi_2Se_4$ pristine slab in Fig.1(d) and 1(e), the large band gap insulator of the $(h\text{BN})_2$ layer is seen to play the same role as the vacuum, i. e. B and N $2p$-states are located far away from the Fermi level and do not disturb the topologically protected interfacial states.

Another important role of hBN is that it opens the possibility to link this system with graphene physics. High quality graphene can be obtained on the hBN substrate[16,17]. Therefore, we design the superlattice structure composed of TI/BI/graphene/BI, which is expected to possess two different Dirac fermions. Atomic configu-

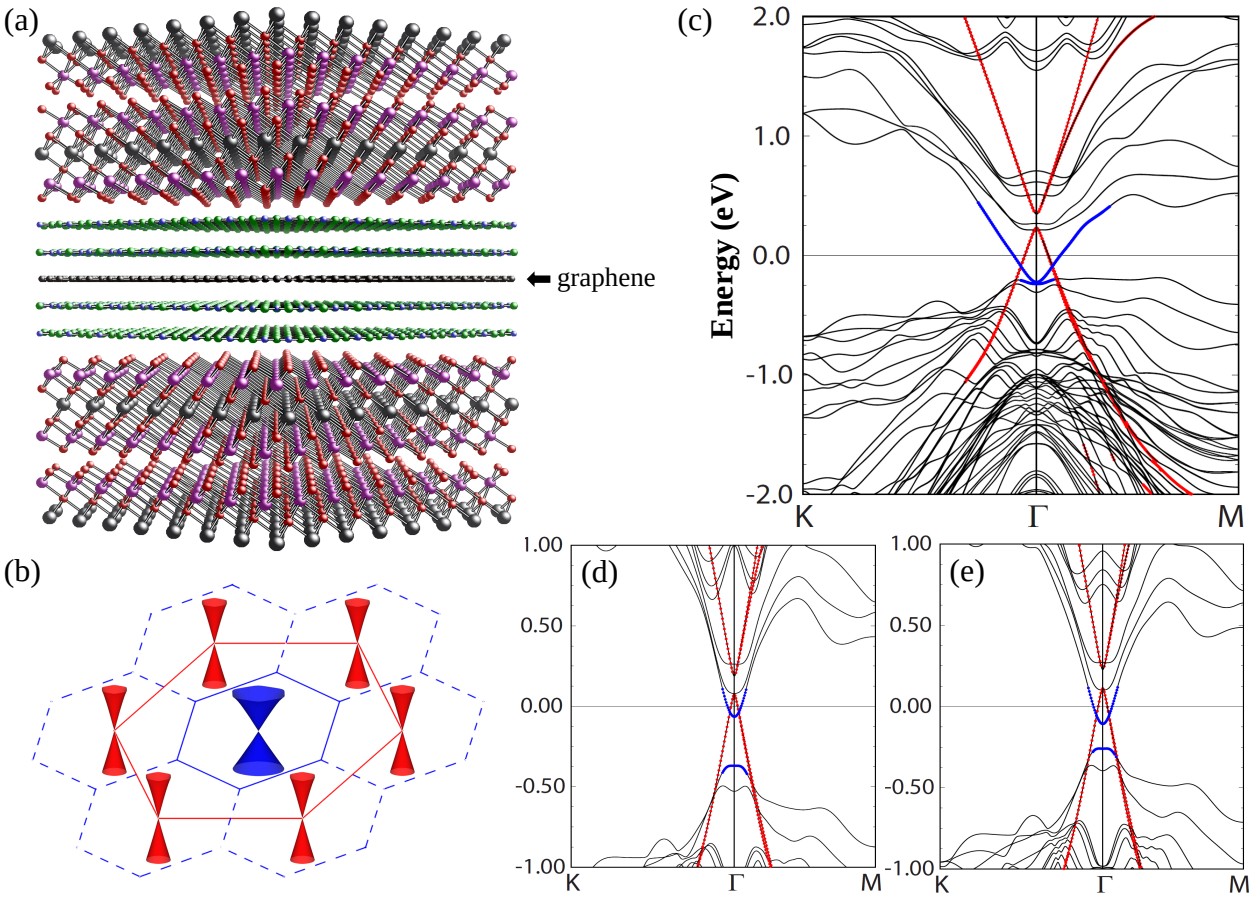

FIG. 2. ((Color Online) a) Crystal structure of the $(PbBi_2Se_4)_3/(hBN)_2/(graphene)_1/(hBN)_2$ superlattice. (b) Red and blue solid hexagons denote the first Brillouin zone of graphene and $PbBi_2Se_4$, respectively, and the blue dotted hexagons correspond to the extended zone of $PbBi_2Se_4$. The K and K′ points of red hexagons are folded into the Γ point of the blue one. Electronic structures of the superlattice depicted in (a) are calculated with (c) full, (d) zero, and (e) half SOC strength, respectively. The energy dispersions with red dots denote graphene Dirac cones and the interfacial Dirac cones are depicted with blue dots.

rations of $(PbBi_2Se_4)_3/(hBN)_2/(graphene)_1/(hBN)_2$ are shown in Fig.2(a), and two kinds of Dirac cones appear in its electronic band structure (Fig.2(c)). The two coexisting Dirac fermions are spatially separated by the $(hBN)_2$ block; thus, they are independent of each other. Because the $\sqrt{3}\times\sqrt{3}$ hexagonal unit cell of hBN and graphene is matched with the 1×1 unit cell of $PbBi_2Se_4$, the original Dirac cones of graphene at the K and K′ points are folded into the Γ point of the smaller hexagonal Brillouin zone of $PbBi_2Se_4$, as shown in Fig.2(b). The different origin of each Dirac cone is revealed when we vary the spin-orbit coupling (SOC) value from 0 to the full strength of the system. As shown in Fig.2(c)-(e), interfacial Dirac cones emerge as the SOC strength increases, whereas the graphene Dirac cones are independent of the variation of SOC. Without SOC, $PbBi_2Se_4$ is a topologically trivial insulator[15], the same as hBN, and the system is identified as a BI/graphene superlattice with only graphene Dirac cones (see Fig.2(d)). As SOC increases up to its original value, $PbBi_2Se_4$ becomes a three-dimensional TI and topologically protected Dirac cones appear in the interfacial region between $PbBi_2Se_4$ and hBN where the band topology is changed spatially.

There are several distinctive features in this multiple Dirac cone system. The Fermi velocity, corresponding to the slope of the linear dispersion, is larger in graphene than in the TI/BI interfacial Dirac cone. And the energy range of the linear dispersion is much wider in graphene because the interfacial Dirac cone mainly exits within the relatively narrow range of the bulk band gap of $PbBi_2Se_4$. There is a mass gap of 0.10eV at the graphene Dirac point, originating from the sublattice symmetry broken by the neighboring hBN layers. The size of the gap is directly related to the interlayer distance between graphene and hBN, which is well-known to be overbound in the local density approximation scheme. The interlayer distance in real systems is expected to be slightly larger than the optimized value. Hence, the real mass gap of the graphene Dirac cone might be smaller due to the decrease of the sublattice asymmetric potential. On the other hand, the interfacial Dirac cone has a gapless feature. Topologically protected interfacial states are robust

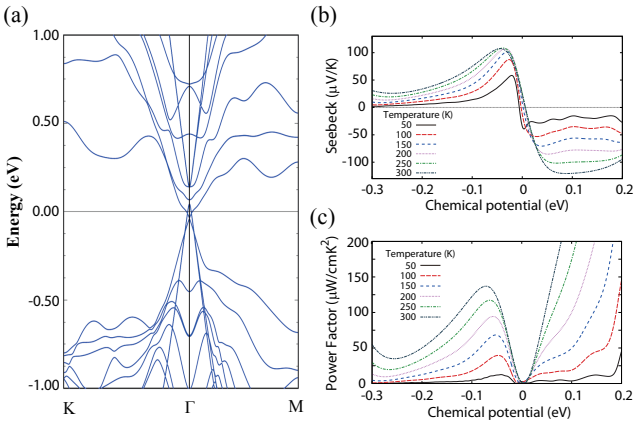

FIG. 3. (Color Online) (a) Band structure of the TI/BI/graphene/BI supperlattice with oxygen substitution of Se near the TI/BI interface. (b) Seebeck coefficients and (c) power factors are calculated as a function of temperature from 50K to 300K.

under the deformation of the interface geometry because the existence of the massless Dirac cone is entirely determined by the topological character of the bulk states away from the interface.

Simultaneously, the TI material has good thermoelectric properties because the heavy elements like Bi or Pb give not only strong spin-orbit effects but also low thermal conductivity[23]. The performance of the thermoelectric material is determined by the figure of merit, $ZT = S^2\sigma T/(\kappa_e + \kappa_L)$, where S is the Seebeck coefficient, σ is the electrical conductivity, and κ_e and κ_L are the electrical and lattice thermal conductivity, respectively. Thus, the low thermal conductivity and the high power factors $S^2\sigma$ are crucial for the high ZT. There have been studies on improving the thermoelectric properties by taking advantage of the topologically protected surface or edge states[24,25]. Also, the multiple copies of the interfacial gapless Dirac cones in the TI/BI superlattice leads to enhancement in the power factors due to the high conductivity of the interfacial Dirac fermions[13], which suggests that the TI/BI superlattice is a good candidate for thermoelectric applications. In the same way, the addition of graphene Dirac cones in the TI/BI superlattice structure gives us strong motivation to investigate possible improvements in thermoelectric properties. As shown in Fig.2(c), the Dirac cones from the graphene layer and the interface between BI and TI contribute to the multiple charge conducting channels around the Fermi level. Moreover, a possible defect formation in $PbBi_2Se_4$ may lead to a decrease of thermal conductivity[26], while the topologically protected interfacial Dirac cones are robust with respect to the non-magnetic defect; this situation resembles the phonon-blocking and electron-transmitting strategy[27].

To investigate the possible enhancement of the thermoelectric properties, we calculated S and σ within the constant relaxation time approximation. Since the locations of the interfacial Dirac cones and the graphene Dirac cones are quite distant (∼0.5eV at the Γ point) as shown in Fig.2(c), we substitute Se at the TI/BI interface by O, which makes the interfacial Dirac cones move upward[13,28]. As a result, the distance between interfacial Dirac cones and graphene Dirac cones decrease to about 0.1eV as shown in Fig.3(a). We here focus on the electronic quasiparticle spectrum in the energy window from -0.3eV to 0.1eV, which is purely composed of two different Dirac cones with the lack of $PbBi_2Se_4$ bulk contributions. The Seebeck coefficients in this energy range show a peak for a small amount of p-type doping. (Fig.3(b)) This peak, originating from the graphene and interfacial Dirac cones, grows as the temperature increases up to 300K. For the calculation of the power factors, we assume 5.7×10^{-13}s for the relaxation time τ to describe the high mobility of the multiple Dirac cones, which is comparable to that of graphene on an SiO_2 substrate whose values are in the range of $10^{-13} \sim 10^{-12}$s[29]. The calculated results in Fig.3(c) show a significant increase, by a factor of approximately 1.5 at 200K for p-type, compared with the previous TI/BI superlattice structure without a graphene layer[13], and become even larger for higher temperatures up to 300K. The abrupt upturn for the positive chemical potential stems from the contribution of the bulk conduction bands. Therefore, the power factors for the p-type doping above -0.3eV of the chemical potential are reliable within our assumption of the relaxation time τ which is set to describe the Dirac cones properly, and the hole carriers through the multiple Dirac cones are responsible for the large enhancement of the power factors in this range of the chemical potential.

We predicted multi-channel Dirac fermions by combining graphene and TI, and constructing superlattice structures. hBN plays an important role to realize multi-Dirac cone materials. On one side, the large gap hBN produces an interface with TI, where there is a jump of Z_2 invariants; on the other side, it glues TI and graphene, in being a good substrate for graphene. Consequently, two independent Dirac cones coexist within a few nanometer thickness and are periodically repeated along the vertical direction. Because all ingredients composing the superlattice basically have a two-dimensional nature and their three-dimensional connections are due to van der Waals type interactions, the proposed geometries are considered to be accessible in experiments and show independent two-dimensional electronic structures from each component. Due to the small thickness of the TI layer, we can minimize the bulk conduction and maximize the conducting channels through the Dirac cones. Moreover, interesting invariants from the superlattice structures are possible. Once we introduce a second graphene layer, the system gives rise to a rich variety of bilayer graphene physics. And there is room for adjusting the interaction strength between two different Dirac fermions by varying the number of hBN layers, i. e. controlling the insulating barrier height. Tunneling through the insulating barrier, exchanging the various degrees of freedom from

each Dirac cone such as spin or pseudospin might be an important experiment.

ACKNOWLEDGMENTS

This paper is dedicated to the memory of Jung-Hwan Song who suffered an untimely death. Financial support from the U.S. DOE under Grant No. DE-FG02-88ER45372 is gratefully acknowledged.

* h-jin@northwestern.edu
† jhsong@pluto.phys.northwestern.edu

[1] A. H. Castro Neto, F. Guinea, N. M. R. Peres, K. S. Novoselov, and A. K. Geim, Rev. Mod. Phys. **81**, 109 (2009).
[2] M. Z. Hasan, and C. L. Kane, Rev. Mod. Phys. **82**, 3045 (2010).
[3] X.-L. Qi, and S.-C. Zhang, ArXiv e-prints 1008.2026, (2010).
[4] J. E. Moore, Nature **464**, 194 (2010).
[5] C. L. Kane, and E. J. Mele, Phys. Rev. Lett. **95**, 146802 (2005).
[6] L. Fu, C. L. Kane, and E. J. Mele, Phys. Rev. Lett. **98**, 106803 (2007).
[7] J. E. Moore, and L. Balents, Phys. Rev. B **75**, 121306 (2007).
[8] R. Roy, Phys. Rev. B **79**, 195322 (2009).
[9] N. M. R. Peres, Rev. Mod. Phys. **82**, 2673 (2010).
[10] P. Roushan, *et al.* Nature **460**, 1106 (2009).
[11] M. König, *et al.* Science **318**, 766 (2007).
[12] A. Rycerz, J. Tworzydlo, and C. W. J. Beenakker, Nature Phys. **3**, 172 (2007).
[13] J.-H. Song, H. Jin, and A. J. Freeman, Phys. Rev. Lett. **105**, 096403 (2010).
[14] K. Watanabe, T. Taniguchi, and H. Kanda, Nature Mater. **3**, 404 (2004).
[15] H. Jin, J.-H. Song, A. J. Freeman, and M. G. Kanatzidis, Phys. Rev. B **83**, 041202 (2011).
[16] C. R. Dean, *et al.* Nature Nanotech. **5**, 722 (2010).
[17] J. Xue, *et al.* Nature Mater. **10**, 282 (2011).
[18] D. Teweldebrhan, V. Goyal, and A. A. Balandin, Nano Lett. **10**, 1209 (2010).
[19] D. Kong, *et al.* Nano Lett. **10**, 2245 (2010).
[20] S. S. Hong, *et al.* Nano Lett. **10**, 3118 (2010).
[21] E. Wimmer, H. Krakauer, M. Weinert, and A. J. Freeman, Phys. Rev. B **24**, 864 (1981).
[22] A. H. MacDonald, W. E. Pickett, and D. D. Koelling, J. Phys. C **13**, 2675 (1980).
[23] T. Tritt, and M. Subramanian, MRS Bulletin **31**, 188 (2006).
[24] R. Takahashi, and S. Murakami, Phys. Rev. B **81**, 161302 (2010).
[25] P. Ghaemi, R. S. K. Mong, and J. E. Moore, Phys. Rev. Lett. **105**, 166603 (2010).
[26] S. Lee, D. Cahill, and R. Venkatasubramanian, Appl. Phys. Lett. **70**, 2957 (1997).
[27] R. Venkatasubramanian, E. Siivola, T. Colpitts, and B. O'Quinn, Nature **413**, 597 (2001).
[28] H. Jin, J.-H. Song, and A. J. Freeman, Phys. Rev. B **83**, 125319 (2011).
[29] Y.-W. Tan, *et al.* Phys. Rev. Lett. **99**, 246803 (2007).